

Electroconvection in homeotropic nematic liquid crystals

NÁNDOR ÉBER* and ÁGNES BUKA

Research Institute for Solid State Physics and Optics,
Hungarian Academy of Sciences, H-1525 Budapest, P.O. Box 49, Hungary

(Received 31 December 2004; in final form 10 February 2005)

Electroconvection is a classical example of pattern-forming phenomena in liquid crystals, typically observed in nematics with negative dielectric and positive conductivity anisotropies. This article focuses on how electroconvection in the homeotropic geometry differs from that in planar alignment. The influence of an additional magnetic field on the pattern characteristics and on secondary instabilities (the normal roll–abnormal roll transition) is discussed. The homeotropic alignment offers unique possibilities also for studying defect motion. Basic characteristics of some patterns of large wavelength are presented and compared with those of the classical Carr–Helfrich structures. Finally, electroconvection in substances with negative conductivity anisotropy is addressed.

Keywords: Electroconvection; Nematic liquid crystal; Homeotropic orientation; Pattern formation

1. Introduction

Anisotropic liquids (e.g. nematic liquid crystals), driven out of equilibrium, offer a rich palette of pattern forming phenomena [1, 2]. Electroconvection (EC) is a classical example of such instabilities [3]. Normally it is observed that if a planarly oriented thin layer of a nematic possessing negative dielectric and positive conductivity anisotropies ($\epsilon_a < 0$, $\sigma_a > 0$) is subjected to an electric field \mathbf{E} normal to the surfaces, when the applied voltage V exceeds a threshold value V_c , the initially homogeneous texture becomes unstable against a periodic tilt modulation of the director associated with flow vortices (convective rolls) and charge separation, resulting in a regular sequence of bright and dark stripes if viewed in a microscope. The ultimate reason for the appearance of the pattern lies in the anisotropy of the electrical conductivity according to the famous Carr–Helfrich mechanism [3–5].

By varying the applied voltage and its frequency f (the two basic control parameters of the system), different pattern morphologies may become observable. There exists a so-called cut-off frequency f_c which divides the frequency range for two distinct electroconvection regimes. In the ‘dielectric’ regime ($f > f_c$) the director is

*Corresponding author. Fax: +36-1-392-22-15. Tel.: +36-1-392-26-30. Email: eber@szfki.hu

oscillating with f , the wavelength Λ of the roll pattern is short ($\Lambda \approx 2\text{--}5\ \mu\text{m}$) and independent of the thickness d of the nematic, and the threshold voltage is proportional to $d\sqrt{f}$. At low frequencies (the ‘conductive’ regime, $f < f_c$), on the contrary, the director distribution is stationary, Λ scales with d , while V_c is independent of the thickness and shows a monotonically increasing, divergence-like behaviour as f approaches f_c .

Usually, in the ‘conductive’ regime there is another morphological transition with frequency at the Lifshitz point f_L . Above the Lifshitz point ($f_L < f < f_c$) the convective rolls are perpendicular to the director (normal rolls, NRs), just as in the ‘dielectric’ regime. However, below f_L the direction of the rolls is rotated by an angle $\pm\beta \neq 0$, with β changing nearly as $\sqrt{(f_L - f)}$, so that one sees a zigzag pattern (oblique rolls, ORs).

During the past decades electroconvection in planar nematics has extensively been studied experimentally, and the proper theoretical description (often referred to as the standard model of EC [3, 6]) has been developed too. Much less attention has been paid to other geometries where the phenomenon can still occur.

In the present article, we review the changes in the characteristics of electroconvection when we use a different initial geometry, namely the homeotropic alignment, without or with an additional magnetic field \mathbf{H} . First we concentrate on the characteristics of the pattern at onset, then we address some questions relating to the behaviour above the threshold (instabilities of the roll pattern); finally we discuss some other pattern morphologies occurring under special conditions (large wavelength patterns and patterns in substances with unusual material parameter combinations).

2. Pattern characteristics at onset

A careful inspection of the Carr–Helfrich mechanism shows immediately that, on switching from the planar initial geometry to a homeotropic one, the torque due to the flow vortices becomes stabilizing. Thus one cannot expect a direct transition from the homogeneous into a patterned electroconvecting state. On the other hand, the dielectric torque becomes destabilizing; thus if the applied voltage exceeds a threshold level V_F , the nematic undergoes a Freedericksz transition, and the director tilts away from the direction normal to the surfaces. Increasing the voltage the tilt angle increases, so the system is getting closer to the planar geometry favoured by the Carr–Helfrich mechanism. As a result EC patterns may appear at a second threshold $V_c > V_F$ as a modulation superposed onto the Freedericksz distorted state, as shown in figure 1(a) [7–9].

In contrast to the planar case, the homeotropic alignment does not have any preferred direction parallel to the surfaces, and the orientation is azimuthally degenerate. The Freedericksz transition breaks this degeneracy, singling out (randomly) a direction for the tilt (which later serves as an already preferred direction for the onset of EC); however, this direction may vary in the sample. Consequently the EC pattern is spatially disordered even at the onset. Moreover, oblique roll patterns always vary with time due to the presence of an inherent torque acting on the rolls; for normal rolls this dynamic disorder starts slightly above V_c [10–14]. This behaviour is a special manifestation of spatio-temporal chaos, called *soft mode turbulence* in order to distinguish it from the usual route to chaos marked

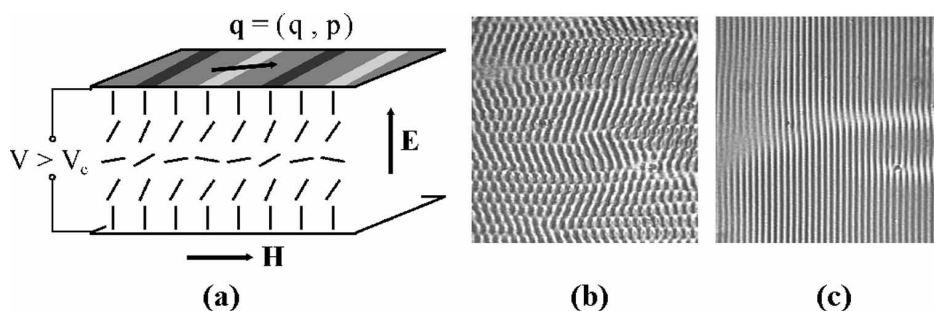


Figure 1. (a) Geometry of the homeotropic electroconvection. (b) Oblique rolls. (c) Normal rolls. Snapshots were taken with polars parallel to \mathbf{H} .

by the generation and violent motion of increasing number of defects as found in the planar EC.

The occurrence of chaos at onset can be easily blocked if one breaks the degeneracy of the orientation by applying a small magnetic field \mathbf{H} parallel to the surfaces [15]. Then the director will tilt towards \mathbf{H} at the Freedericksz transition and the EC rolls appearing at $V > V_c$ will be nicely ordered too, exhibiting the same pattern morphologies found in planar samples (see figures 1b and 1c).

The aim of our experimental studies was to explore how the magnetic field strength affects the characteristics of the EC pattern. The measurements were carried out using a standard nematic mixture (Phase 5A, Merck), which allowed access to the ‘conductive’ regime in a wide frequency range. The pattern was observed with a long-range microscope using either a single polarizer (shadowgraph technique) or crossed polarizers [16]. The EC threshold voltage exhibited the usual increase with the frequency for any magnetic field, as expected. While studying the magnetic field dependence of V_c , however, a non-monotonic behaviour was detected at low frequencies [17], in contrast to the monotonic increase of $V_c(H)$ found for higher f as shown in figure 2(a).

This behaviour can be explained as follows. Though at low f the EC threshold voltage is the lowest, $V_c > V_F$ must always hold, as a minimum tilt angle is required for the Carr–Helfrich mechanism to work. The magnetic field tends to orient the director parallel to \mathbf{H} , hence the field reduces the Freedericksz threshold voltage. Then the required tilt can be realized at lower voltages; thus $V_c(H)$ follows the trend of $V_F(H)$ for small fields. At higher H , however, the further increase of the tilt at the same time suppresses the modulation of the tilt, so V_c must increase. For high frequencies $V_c \gg V_F$, consequently one has already a quasiplanar structure at the onset, thus the stabilizing effect of the magnetic field dominates in the full H range.

The in-plane wavevector of the pattern $\mathbf{q} = (q, p)$ was measured too [16–19]. Figure 2(b) shows the obliqueness $p/q = \tan \beta$ of the convection rolls versus f and H . It depicts an unusual morphological transition for small H , and the reappearance of normal rolls ($p = 0$) at diminishing frequencies. Such a transition has neither been reported for planar cells, nor for homeotropic samples of other nematics. Theoretical calculations have confirmed that the material parameter set (elastic moduli, viscosities, etc.) of Phase 5A allows for the presence of two Lifshitz points [17, 18], while for other sets (e.g. for N-(*p*-methoxybenzilidene)-*p*-butylaniline, MBBA) the

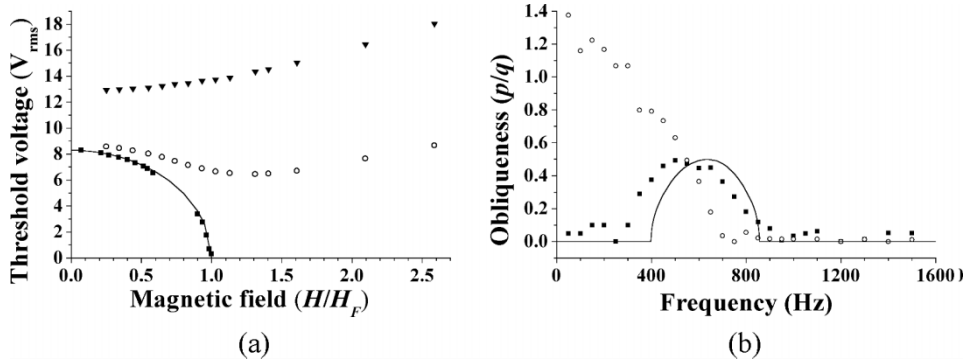


Figure 2. (a) Magnetic field dependence of the threshold voltage for the Fredericksz transition (measured: solid squares, calculated: solid line) and for the electroconvection at $f=50$ Hz (open circles) and at $f=800$ Hz (solid triangles). (b) The frequency dependence of the obliqueness (p/q) of the EC roll pattern for small ($H=0.249H_F$, solid squares) and high ($H=1.028H_F$, open circles) magnetic field. The solid line is the theoretical prediction for a small ($H=0.32H_F$) magnetic field. H_F is the magnetic Fredericksz threshold field at $V=0$.

usual single Lifshitz point has been obtained. At increasing magnetic field the Lifshitz point(s) are shifting towards lower frequencies, so the regular behaviour with one f_L is recovered.

3. Behaviour above the EC threshold

When electroconvection is studied at applied voltages above V_c , it is convenient to introduce a dimensionless control parameter $\varepsilon = (V^2 - V_c^2)/V_c^2$ which characterizes the relative deviation from the threshold. For $\varepsilon > 0$ the morphology of the pattern may change and further instabilities may reduce or destroy the initial order of the convection rolls.

One example of such instabilities is the transition from NR to AR (abnormal roll). While \mathbf{q} is the same for both AR and NR, in ARs the director rotates away from its initial direction along \mathbf{H} [20]. Theoretical explanation of the phenomenon can be given using a weakly nonlinear description (Ginzburg–Landau equations, GLE) based on the recognition that the pattern amplitude (the tilt modulation) may be coupled to the azimuthal angle φ of the director. While at the onset ($\varepsilon=0$) and for small ε values, $\varphi=0$, if ε exceeds a critical value $\varepsilon_{AR} > 0$ it allows for a symmetry breaking in the form of a forward bifurcation (the NR–AR transition), leading to an azimuthal angle $\varphi = \pm\Phi\sqrt{\varepsilon - \varepsilon_{AR}}$ continuously increasing with ε [21, 22].

Though this NR–AR transition is not an exclusive feature of the homeotropic alignment (it has also been observed in planar samples), the azimuthal degeneracy of the homeotropic alignment offers an easier detection, as $\varphi \neq 0$ means a net rotation of the optical axis of the sample [23]. While NR and AR look very similar when viewed with light polarized parallel to \mathbf{H} , they can be distinguished if one breaks the left–right symmetry by rotating the polarizer by an angle $\alpha \neq 0$. Experiments have shown that ARs form domains with $\varphi < 0$ and $\varphi > 0$ with a smooth variation of φ between the domains [16, 19]. These domains form a secondary (quasi)periodic structure of large wavelength for $\varepsilon \gg \varepsilon_{AR}$.

We have also developed another method based on digital image processing for the visualization of the abnormal rolls [16, 18, 19]. Snapshots of the pattern were taken with a CCD camera at various polarizer settings, i.e. while increasing α in equidistant steps. The same selected row of subsequently digitized images was copied at video rate into the subsequent rows of a new image. The resulting x - α image demonstrates how the transmitted intensity depends on the polarizer angle, as well as on the spatial direction normal to the rolls. Figures 3(a) and (b) show the x - α images of NR and AR, respectively, using crossed polarizers. This method allows a quantitative determination of the azimuthal angle. Measuring $\varphi(\varepsilon)$ the theoretical prediction for a forward pitchfork bifurcation could be justified [16, 18, 19], as shown in figure 4. Moreover, the measured frequency dependence of the parameter Φ characterizing the opening angle of the pitchfork exhibited a divergence when approaching the Lifshitz point, in agreement with the theory [18]. The expected $\varepsilon \propto H^2$ dependence of the threshold of the NR-AR transition could also be proved [17].

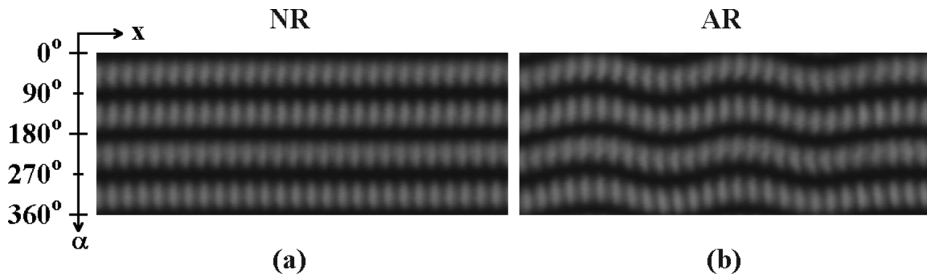


Figure 3. x - α images of (a) normal rolls and (b) abnormal rolls taken with crossed polars (α is the angle of the polarizer made with \mathbf{H}). Extinction occurs if the polarizer is parallel or perpendicular to the director. The curvature of the extinction lines indicates spatial variation of the azimuthal angle of the director.

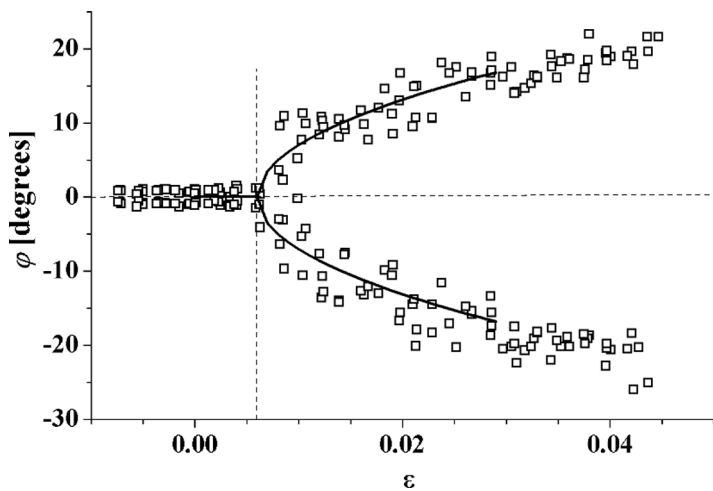


Figure 4. ε dependence of the azimuthal angle φ of the director at the NR-AR transition. Open squares denote the measured points, solid lines represent a least squares fit yielding $\varepsilon_{AR} = 0.006$ and $\Phi = 110^\circ$. $f = 1000$ Hz, $H = 0.26H_F$.

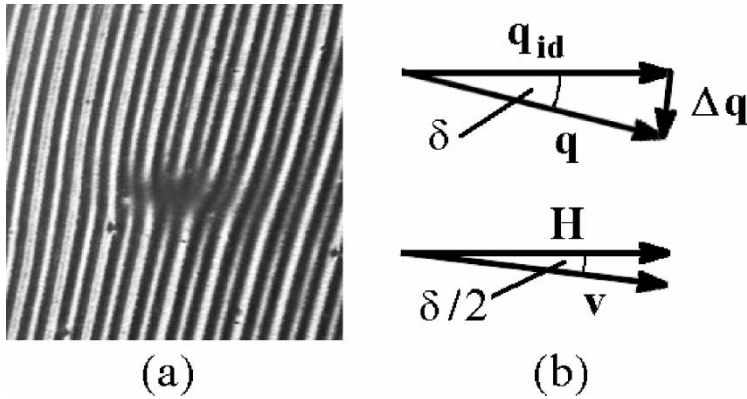


Figure 5. (a) Snapshot of a defect in a roll pattern (image taken after rotating the cell by an angle δ in the magnetic field). (b) Directions of the wavevectors and the defect velocity for the same geometry.

Besides the NR–AR transition there are other possibilities for the ordered roll pattern to become unstable. The most common example is the appearance of defects (dislocations). Generally defects play an important role in adjusting the proper wavevector if – e.g. after a sudden change – the actual \mathbf{q} of the pattern does not match the ideal one (\mathbf{q}_{id}) belonging to the actual values of the control parameter(s). The relaxation of the pattern to \mathbf{q}_{id} occurs via generation and motion of defects. Motion along the rolls (climb) modifies $|\mathbf{q}|$, while motion normal to the rolls (glide) changes the direction of \mathbf{q} . The GLE mentioned earlier can provide a solution for the motion of a single defect, predicting a defect velocity \mathbf{v} perpendicular to the wavevector mismatch $\Delta \mathbf{q} = \mathbf{q} - \mathbf{q}_{id}$ as well as a logarithmic divergence of $|\mathbf{v}|$ when $|\Delta \mathbf{q}| \rightarrow 0$. The homeotropic geometry offers an easy way to create a wavevector mismatch by simple rotation of the cell (and the pattern) in the magnetic field by an angle δ (see figure 5). In this case the defect motion is mainly a glide with a little climb component. The measurements on Phase 5A and on MBBA proved both $\mathbf{v} \perp \Delta \mathbf{q}$ and the logarithmic behaviour [24].

4. Patterns of large wavelength

The wavelength of the EC roll pattern in the ‘conductive’ regime is typically $\Lambda \approx (0.5-1.5)d$, and it is even less in the ‘dielectric’ regime (for the usual sample thicknesses $d > 10 \mu\text{m}$). Nevertheless, occasionally one can observe patterns with much larger wavelength than that of the rolls. The abnormal roll domains (figure 6a) mentioned above serve as an example [19].

Another classical representative is the chevron pattern which is mainly seen in the ‘dielectric’ regime. It again represents a superstructure, where the direction of the convective rolls as well as that of the director (being normal to the rolls) alternate in the neighbouring domains, resulting in a zigzag structure. The domains are separated by ordered chains of defects (dislocations), indicating that this pattern occurs at fairly high ε values. It has been shown [19], however, that chevrons are not an exclusive feature of the ‘dielectric’ regime; they could be observed also in the ‘conductive’ regime of homeotropic samples without (or with small enough) magnetic

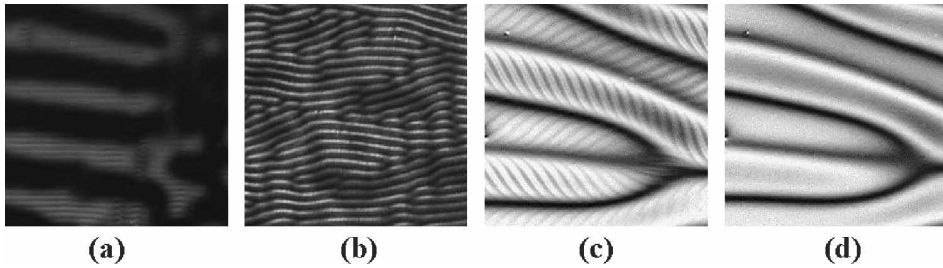


Figure 6. Snapshots of large wavelength patterns in homeotropic nematics. (a) Abnormal roll domains (crossed polars, $\alpha = 8^\circ$). (b) Chevron pattern in the ‘conductive’ regime (parallel polars, $\alpha = 0^\circ$). (c) ‘Defect free’ chevron (crossed polars, $\alpha = 0^\circ$). (d) ‘Prewavy’ pattern (crossed polars, $\alpha = 0^\circ$).

field (figure 6b). A higher magnetic field seemed to suppress the tendency of the defects ordering into chains.

Recently another type of chevrons – the ‘defect free’ chevrons [25] – has also been identified in the ‘conductive’ regime. Though their main characteristics are very similar to the ordinary – ‘defect mediated’ – chevrons, there are no defects at the domain boundaries; rather the rolls seem to have a curvature (figure 6c). Reducing the applied voltage in the presence of ‘defect free’ chevrons, the rolls disappear but a pattern with a large wavelength (called ‘prewavy’ pattern [26], PWP, figure 6d) persists for some voltage range. The ‘prewavy’ pattern is characterized by an azimuthal modulation of the director, as opposed to the tilt modulation in the EC rolls. Consequently the PWP produces no shadowgraph image; it can be observed with crossed polarizers only. PWP can exist in a wide frequency range, even at f much above the cut-off. The frequency dependence of the threshold voltage is nearly linear, definitely weaker than either in the ‘conductive’ or in the ‘dielectric’ regime. The voltage dependence of the azimuthal angle in PWP exhibits a pitchfork-like bifurcation [27], similar to that at the NR–AR transition. Up to now PWP has been observed in nematics with high electrical conductivity only. With proper adjustment of the conductivity one can obtain ‘conductive’ rolls, ‘dielectric’ rolls and the ‘prewavy’ pattern in a sequence in the same cell when increasing the frequency, as shown in figure 7. For samples with higher electrical conductivity (e.g. at higher temperature), usually the ‘conductive’ rolls switch to PWP directly at a frequency f_{pw} [28]. The ‘defect free’ chevrons are actually observed at frequencies slightly above f_{pw} indicating that they are a superposition of two patterns, the PWP and the normal rolls. From the above observations one can conclude that the formation of the PWP is not due to the Carr–Helfrich mechanism, but unfortunately its actual mechanism has remained unexplored yet.

5. Substances with $\sigma_a < 0$

Though for most nematics $\sigma_a > 0$ there are a few compounds – some of those having a smectic phase below the nematic – which possess $\sigma_a < 0$ in some temperature range. The Carr–Helfrich mechanism stops working for substances with $\varepsilon_a < 0$ if $\sigma_a \rightarrow 0$ or becomes negative. However, if a substance has $\varepsilon_a > 0$ and $\sigma_a < 0$ (i.e. the signs of both anisotropies are inverted compared to the standard electroconvecting nematics)

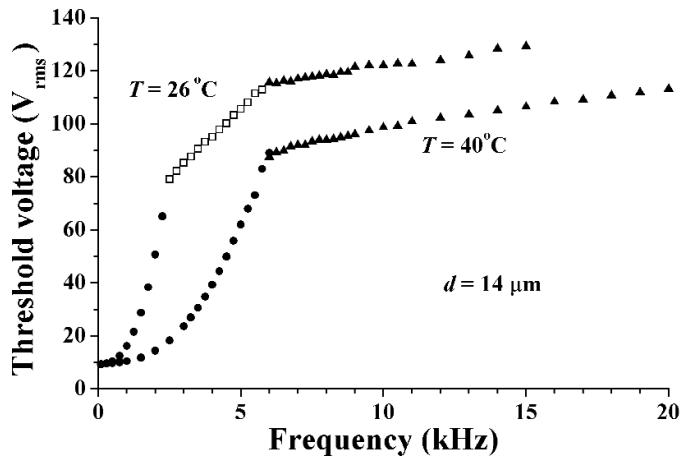


Figure 7. Frequency dependence of the threshold voltages for various EC patterns in a mixture of Phase 5 and Phase 5A. Solid squares, open circles and solid triangles correspond to the ‘conductive’ rolls, the ‘dielectric’ rolls and the ‘prewavy’ pattern respectively.

and additionally we start from the homeotropic initial state (instead of the planar one), the Carr–Helfrich mechanism becomes operational again, and a direct transition from the uniformly oriented to the patterned state can be observed [29, 30]. The peculiarity of this transition is that the azimuthally isotropic symmetry of the homeotropic alignment is broken during the appearance of the EC pattern, which is in contrast to the classical case discussed in the previous sections, where it occurred already at the Freedericksz transition preceding the onset of EC. As a result, the morphology of the patterns is different; rolls exist only at low frequencies, while at higher f various types of square grid patterns are observed. It has been shown that these morphological variations as well as the frequency dependence of the threshold voltages can be satisfactorily described theoretically by the standard model of EC [31].

6. Conclusions

We surely could not give a full coverage of all phenomena related to homeotropic electroconvection in the present review; yet the results shown above provide examples for the two typical scenarios occurring as a consequence of changing the initial alignment.

On the one hand, there are features where no qualitative change of the behaviour is observed. We have mostly the same morphological transitions when frequency or voltage is varied; however, the threshold voltages or the Lifshitz point differ quantitatively (e.g. the threshold ε_{AR} for the NR–AR transition is about an order of magnitude smaller in homeotropic cells than in a planar one).

On the other hand, some features are closely connected to the homeotropic alignment, either through the splay-bend Freedericksz distorted state preceding the onset of electroconvection (as the re-entrant low frequency NRs and the minimum in the $V_c(H)$ curve), or via the azimuthal degeneracy of the alignment (e.g. chaos at onset).

The most challenging field is, however, electroconvection in homeotropically aligned nematics of $\sigma_a < 0$, where the translational invariance and the isotropic in-plane symmetry of the orientation should break simultaneously at the onset, thus requiring an unusual theoretical treatment.

Acknowledgements

Fruitful discussions with L. Kramer, W. Pesch, A. G. Rossberg, S. Kai, Y. Hidaka, J.-H. Huh and T. Tóth Katona are gratefully acknowledged. This work was partially supported by the Hungarian Research Grants OTKA T 037336, M 041888 and NKFP-128/6 as well as by the EU Research Training Network PHYNECS. N.É. is grateful to the hospitality provided by the Ewing Christian College, Allahabad, within the framework of a bilateral exchange project of the Indian National Science Academy and the Hungarian Academy of Sciences.

References

- [1] A. Buka and L. Kramer (Editors), *Pattern Formation in Liquid Crystals* (Springer-Verlag, New York, 1996).
- [2] Á. Buka, T. Börzsönyi, N. Éber and T. Tóth-Katona, Patterns in the bulk and at the interface of liquid crystals. *Lecture Notes in Physics* **567** 298–318 (2001)
- [3] L. Kramer and W. Pesch, Electrohydro-dynamic Instabilities in Nematic Liquid Crystals, in *Pattern Formation in Liquid Crystals*, edited by A. Buka and L. Kramer (Springer-Verlag, New York, 1996) pp. 221–256.
- [4] S. Chandrasekhar, *Liquid Crystals* (Cambridge University Press, Cambridge, 1992).
- [5] P.G. de Gennes and J. Prost, *The Physics of Liquid Crystals* (Clarendon Press, Oxford, 1993).
- [6] E. Bodenschatz, W. Zimmermann and L. Kramer, *J. Phys. (France)* **49** 1875 (1988).
- [7] D. Meyerhofer and A. Sussman, *Appl. Phys. Lett.* **20** 337 (1972).
- [8] M.I. Barnik, L.M. Blinov, M.F. Grebenkin, S.A. Pikin and V.G. Chigrinov, *J. Exp. Theor. Phys. (URSS)* **69** 1080 (1975).
- [9] H. Richter, A. Buka and I. Rehberg, *Mol. Cryst. Liq. Cryst.* **251** 181 (1994).
- [10] H. Richter, A. Buka and I. Rehberg, *Phys. Rev.* **E51** 5886 (1995).
- [11] S. Kai, K. Hayashi and Y. Hidaka, *J. Phys. Chem.* **100** 19007 (1996).
- [12] Y. Hidaka, J.-H. Huh, K. Hayashi, M. Tribelsky and S. Kai, *J. Phys. Soc. Japan* **66** 3329 (1997).
- [13] Y. Hidaka, J.-H. Huh, K. Hayashi, S. Kai and M. Tribelsky, *Phys. Rev.* **E56** R6256 (1997).
- [14] P. Tóth, Á. Buka, J. Peinke and L. Kramer, *Phys. Rev.* **E58** 1983 (1998).
- [15] H. Richter, N. Kloepper, A. Hertrich and Á. Buka, *Europhys. Lett.* **30** 37 (1995).
- [16] N. Éber, A.G. Rossberg, Á. Buka and L. Kramer, *Mol. Cryst. Liq. Cryst.* **351** 161 (2000).
- [17] N. Éber, Sz. Németh, A.G. Rossberg, L. Kramer and Á. Buka, *Phys. Rev.* **E66** 036213 (2002).
- [18] A. G. Rossberg, N. Éber, Á. Buka and L. Kramer, *Phys. Rev.* **E61** R25 (2000).
- [19] Á. Buka, P. Tóth, N. Éber and L. Kramer, *Physics Reports* **337** 157 (2000).
- [20] H. Richter, A. Buka and I. Rehberg, *Mol. Cryst. Liq. Cryst.* **251** 181 (1994).
- [21] A.G. Rossberg, A. Hertrich, L. Kramer and W. Pesch, *Phys. Rev. Lett.* **76** 4729 (1996).
- [22] A.G. Rossberg and L. Kramer, *Physica Scripta* **T67** 121 (1996).
- [23] J.-H. Huh, Y. Hidaka and S. Kai, *Phys. Rev.* **E58** 7355 (1998).
- [24] P. Tóth, N. Éber, T.M. Bock, Á. Buka and L. Kramer, *Europhys. Lett.* **57** 824 (2002).
- [25] J.-H. Huh, Y. Hidaka, A.G. Rossberg and S. Kai, *Phys. Rev.* **E61** 2769 (2000).
- [26] S. Kai and K. Hirakawa, *Solid State Commun.* **18** 1573 (1976).
- [27] J.-H. Huh, Y. Hidaka, Y. Yusril, N. Éber, T. Tóth-Katona, Á. Buka and S. Kai, *Mol. Cryst. Liq. Cryst.* **364** 111 (2001).

- [28] N. Éber, S. Németh, T. Tóth-Katona, Á. Buka and L. Kramer, paper presented at the *International Conference on Pattern Formation and Self-organization in Nonlinear Complex Systems*, Beijing, 11–16 June (2001).
- [29] Á. Buka, B. Dressel, W. Otowski, K. Camara, T. Tóth-Katona, L. Kramer, J. Lindau, G. Pelzl and W. Pesch, *Phys. Rev.* **E66** 051713 (2002).
- [30] Á. Buka, B. Dressel, L. Kramer and W. Pesch, *Chaos* **14** 793 (2004).
- [31] Á. Buka, B. Dressel, L. Kramer and W. Pesch, *Phys. Rev. Lett.* **93** 044502 (2004).